

Analytical modeling and parameter estimation of photovoltaic strings under partial shading conditions

Jieming Ma ^{a,b,*}, Dou Hong ^{a,b}, Kangshi Wang ^{a,b}, Ziqiang Bi ^{a,b}, Xiaohui Zhu ^{a,b}, Jie Zhang ^{a,b}

^a School of Advanced Technology, Xi'an Jiaotong-Liverpool University, 111 Ren'ai Road, Suzhou, 215123, Jiangsu, PR China

^b Department of Computer Science, University of Liverpool, Brownlow Hill, Liverpool, L69 3BX, UK



ARTICLE INFO

Keywords:

Photovoltaic cells

Simulation

Modeling

Parameter estimation

Partial shading conditions

ABSTRACT

An accurate estimation of the photovoltaic (PV) electrical characteristics is of significance to the decision-making related to the establishment and operation of PV systems. However, most of the existing PV models are very limited to predicting the PV behaviors under uniform irradiation conditions (UICs). This paper proposes a complete solution to modeling and simulation of PV strings under partial shading conditions (PSCs). The measured current-voltage ($I-V$) data are first characterized by a shading information matrix containing essential environmental conditions for operating points. The model parameters are estimated via a four-state Jaya (FSJ) algorithm, which applies an exploration-exploitation adaptation mechanism to make an appropriate trade-off between global and local searching efforts. Fed by the obtained shading information and optimal parameters, the “staircase” shape $I-V$ curve can be accurately predicted via a comprehensive analytical PV model. The experimental results are tested on two different PV strings with multi-crystalline and mono-crystalline PV technologies. Results suggest that the proposed FSJ algorithm outperforms reported state-of-the-art optimization algorithms in terms of convergence speed and prediction errors. With the optimal parameters, the analytical PV model gives superior results under various PSCs. The proposed model and algorithms can serve as an efficient alternative for modeling PV strings.

1. Introduction

The development of photovoltaic (PV) energy is becoming a focal point and many countries devote considerable resources to the research PV systems [1,2]. Owing to the high initial cost, the optimal utilization of the available PV energy should be ensured [3]. A simple and accurate PV model, which has the capability of estimating the PV electrical characteristics towards a variety of operating conditions, is of significance in the design and development phases [4].

Over the years, a good number of researchers have studied the modeling and simulation methods of PV systems [4–6]. A popular modeling approach is to analyze the current-voltage ($I-V$) or power-voltage ($P-V$) characteristics by utilizing the equivalent circuit. The single-diode model (SDM), comprising a linear independent current source and a diode, is the most widely used circuit-based PV model featured with its simplicity [5]. An improved model is done by the inclusion of a series resistance and a shunt resistance [7], but significant computing effort is required to extract model parameters. To simplify

the computation in simulation, Ma et al. [4] introduced an iteration-free SDM, but the accuracy deteriorates in the vicinity of the open-circuit voltage, especially at a low irradiance level. In an attempt to consider the recombination loss at the space depletion region of PV cells, a double-diode model (DDM) was developed to better express PV cell behavior [8]. In view of the recombination in the defect regions, grain sites, etc., a third diode can be added in parallel to the two diodes of DDM, and the model is named triple-diode model or three-diode model (TDM) in the literature [9]. Although the DDM and TDM have certain advantages, the extra diodes increase more unknown model parameters. Moreover, most of the existing circuit-based PV models are limited to predicting PV behaviors under a uniform irradiation condition (UIC).

Recent studies have shown that a PV string exhibits strongly nonlinear $I-V$ characteristics when one or more PV cells receive lower radiation than the others. It is called partial shading condition (PSC) in the literature [10]. Under PSCs, a PV string obtains “staircase” shape $I-V$ characteristics, bringing many challenges for modeling. Empirical methods are not based on circuit-based models but utilize empirical

* Corresponding author. School of Advanced Technology, Xi'an Jiaotong-Liverpool University, 111 Ren'ai Road, Suzhou, 215123, Jiangsu, PR China.

E-mail addresses: jieming84@gmail.com (J. Ma), dou.hong16@student.xjtu.edu.cn (D. Hong), kangshi.wang19@student.xjtu.edu.cn (K. Wang), bzq2810@outlook.com (Z. Bi), Xiaohui.Zhu@xjtu.edu.cn (X. Zhu), Jie.Zhang01@xjtu.edu.cn (J. Zhang).

equations and a set of parameters to evaluate the relation of the output characteristics [11]. Many empirical methods correlate the irradiance and ambient temperature to the electrical characteristics of a PV system. In Refs. [12,13], the modeling methods are integrated with the irradiance model. Although they can estimate output power under PSCs, many of these models cannot predict every operating point of the I–V curve. Moreover, Empirical methods often offer simple empirical equations, so they are simple, convenient, and easy to calculate and use. However, a number of assumptions and simplifications are utilized in these equations, which indicate the theoretical foundation is not solid. They can roughly estimate the output characteristics but there is no guarantee that high-accuracy estimation can be achieved. Like empirical methods, machine learning-based methods avoid circuit-based PV models, and no prerequisite knowledge of PV devices is required. In Ref. [14], the maximum available power of PV arrays is predicted via an artificial neural network (ANN), in which the irradiance, solar angles, and ambient temperature are used as input variables of ANN. Kanwal et al. [15] proposed support vector machine (SVM) and Gaussian process regression (GPR) models for output power prediction and maximum power point estimation in ambient weather. According to their simulation results, the SVM-based trained model obtains higher prediction accuracy than the GPR model. In Ref. [16], the I–V or P–V curves are generated via an adaptive-network-based fuzzy inference system (ANFIS). The machine learning method has the ability to provide accurate and reliable estimations if the training data are well prepared. However, it is hard to collect the data covering all PSCs. In addition, the models have to be re-trained if performance degradation occurs in the PV system.

Regardless of PV models, a parameter estimation method is crucial for designing and simulating the optimal PV system behavior [17]. The most classical approaches are deterministic algorithms, such as Newton Raphson [18] and nonlinear least-squares optimization [19]. They perform extremely well for smooth unimodal problems. When a complicated PV model is applied in the objective function, a large deviation between the measured and the estimated I–V characteristics can be detected [20]. Compared to deterministic algorithms, stochastic algorithms are computationally efficient. They include Jaya algorithm [21], simulated annealing (SA) [22], particle swarm optimization (PSO) [23,24], differential evolution (DE) [25], pattern search [26], flower pollination algorithm (FPA) [20,27], Rao-based chaotic optimization (RCO) [28], cuckoo search (CS) [29], bacterial foraging (BF) [30], harmony search (HS) [31], marine predators algorithm (MPA) [32], chaotic whale optimization algorithm (CWOA) [33], teaching–learning–based artificial bee colony (TL-ABC) [34], multiple learning backtracking search algorithm (MLBSA) [35], imperialist competitive algorithm (ICA) [36], etc. These algorithms have the ability to describe complex relationships and work well in the SDM and DDM, but their optimization performance mainly depends on the initial values and default hyperparameters. In addition, they were not examined to extract the optimal parameters under different PSCs.

This paper proposes a complete solution for modeling and simulation of PV strings operating under UICs and PSCs. To show the proposed model's superiority, it is applied to predict the I–V characteristic curves for two different PV modules under a variety of complex environmental conditions. Also, the proposed method's accuracy is compared with that of commercial PV simulation tools. The main contributions of this paper are summarized as follows:

- A shading information extraction method is introduced to arrange environmental conditions and bypass diode configurations of a PV string.

- An analytical modeling method is proposed to predict a PV string's current under PSCs.
- A four-state Jaya (FSJ) algorithm improves the model's accuracy using appropriate explorative-exploitative behaviors.

The desired model would be a useful tool for researchers to predict the output characteristics of a PV generator under both UICs and PSCs. It aids in PV installation planning and development without going into the low-level technical details. Furthermore, the PV model can be used to study and evaluate the effectiveness of maximum power point tracking (MPPT) techniques for partially shaded PV systems.

The rest of this paper is organized as follows: In Section 2, the PV SDM and its behavior under PSC are introduced. Section 3 demonstrates problem formulation and parameter estimation for the proposed analytical PV model. Section 4 discusses the experimental results and their comparison with the existing simulation tools. Lastly, Section 5 provides the conclusion to this work.

2. Electrical characteristics of a photovoltaic string

2.1. Single-diode photovoltaic model

The process of generating electricity upon exposure to light is called PV effect, which is the basic working principle of PV cells. A simple method of representing the PV cell current I_C is to assume that the superposition principle holds – the overall I–V characteristic is the sum of the dark and illuminated characteristics [37]. When a PV cell is exposed to light, it can be modeled by a linear independent current source, a series resistor R_s and a shunt resistor R_p . The PV cell behaves like a diode without the PV effect. Therefore, the overall I–V characteristics of a PV cell can be expressed by an SDM as shown in Eq. (1) [38].

$$I_C = I_{ph} - I_o \left[\exp\left(\frac{V_D}{AV_t}\right) - 1 \right] - \frac{V_D}{R_p} \quad (1)$$

where I_o is the reverse saturation current; I_{ph} is the light-generated current; and A is the ideality factor of the diode. The thermal voltage of the cell is denoted as V_t , which can be estimated as a function of cell temperature T : $V_t = kT/q$, where k is the electron charge and k is the Boltzmann's constant. According to Kirchhoff's voltage law, the voltage drop across the diode V_D can be calculated by $V_D = V_C + I_C R_s$, where V_C is the PV terminal voltage.

The photo-generated current I_{ph} increases nearly linearly with the irradiance levels, and it can be mathematically expressed by Eq. (2) [39].

$$I_{ph} = (I_{phn} + K_I \Delta T) \frac{G}{G_n} \quad (2)$$

The difference between T and T_n is ΔT which also affects the value of I_{ph} . In Eq. (2), K_I is the short-circuit current coefficient. The I_{phn} denotes the light-generated current at the standard test conditions (STCs): radiation of $G_n = 1.0 \text{ kW/m}^2$, and a cell temperature of $T_n = 25^\circ\text{C}$ at 1.5 air mass spectral distributions. We can assume that $I_{phn} = I_{scn}$ to simplify the model. In Ref. [6], Villalva et al. proposed an expression determining the dependence of reverse saturation current on the temperatures:

$$I_o = \frac{I_{scn} + K_V \Delta T}{\exp((V_{ocn} + K_V \Delta T)/AV_t) - 1} \quad (3)$$

where V_{ocn} and I_{scn} are the open-circuit voltage and short-circuit current at STCs, respectively. The K_V is the open-circuit voltage coefficient.

A PV-cell string is basically series-connected PV cells. Let N_S represent the number of PV cells in a string. The string current-string voltage

(I_S-V_S) relations can be rewritten as:

$$I_S = I_{ph} - I_o \left[\exp\left(\frac{V_D}{AN_S V_t}\right) - 1 \right] - \frac{V_D}{R_p} \quad (4)$$

where $V_D = V_C + I_C R_S$. Uniform irradiation is referred to a condition that PV cells or strings revive a fixed intensity level of light. Under UICs, the P-V characteristic curves present a unique maximum power point.

2.2. Partial shading conditions

The entire PV string receives non-uniform irradiation under PSCs. Fig. 1(a) shows two separated PV cells at two different irradiance levels ($G_1 = 0.4 \text{ kW/m}^2$, $G_2 = 1.0 \text{ kW/m}^2$). The overall current sinks strongly, and the shaded cell C_1 absorbs electric power generated by C_2 . The electrical energy is then converted into heat energy and may damage the shaded C_1 . This phenomenon is called the “hot-spot”. The bypass diode is a necessary component used to protect against “hot spots” and reduce power losses caused by PSCs. Fig. 1(b) shows the same PV string with two bypass diodes (B_1 and B_2). Three turning points (TPs) divide the entire $I-V$ curve into two regions. In Region 1, the isolated C_2 is firstly

activated with the starting short-circuit current I_{sc1} . The PSC leads to the activation of bypass diode B_1 , which diverts the current away from the shaded cell, resulting in a two-step current waveform. When the current decreases to the second current step, both cells work in Region 2 and no bypass diode is activated. For i th ($i = 1, 2, 3, \dots$) region, the I_S-V_S relations can be mathematically expressed by Eq. (5).

$$I_S = I_{ph,i} - I_{o,i} \left[\exp\left(\frac{V_{D,i}}{A_i N_{S,i} V_{t,i}}\right) - 1 \right] - \frac{V_{D,i}}{R_{p,i}}, V_{tp,i} \leq V_S < V_{tp,i+1}, \quad (5)$$

where $V_{D,i} = V_C + I_C R_S$. The $V_{tp,i}$ represents the voltage of the i th TP. The “staircase” shape $I-V$ curve leads to a multiple-peak P-V curve. Among many local power peaks, the one generating maximum power is the global maximum power point (GMPP).

In summary, the following observations (OBSS) can be made from the $I-V$ characteristic curves of PV strings under PSCs:

OBS1: the $I-V$ characteristics are not tied to shaded position in the string but rather to the number of shaded cells and bypass diode configurations;

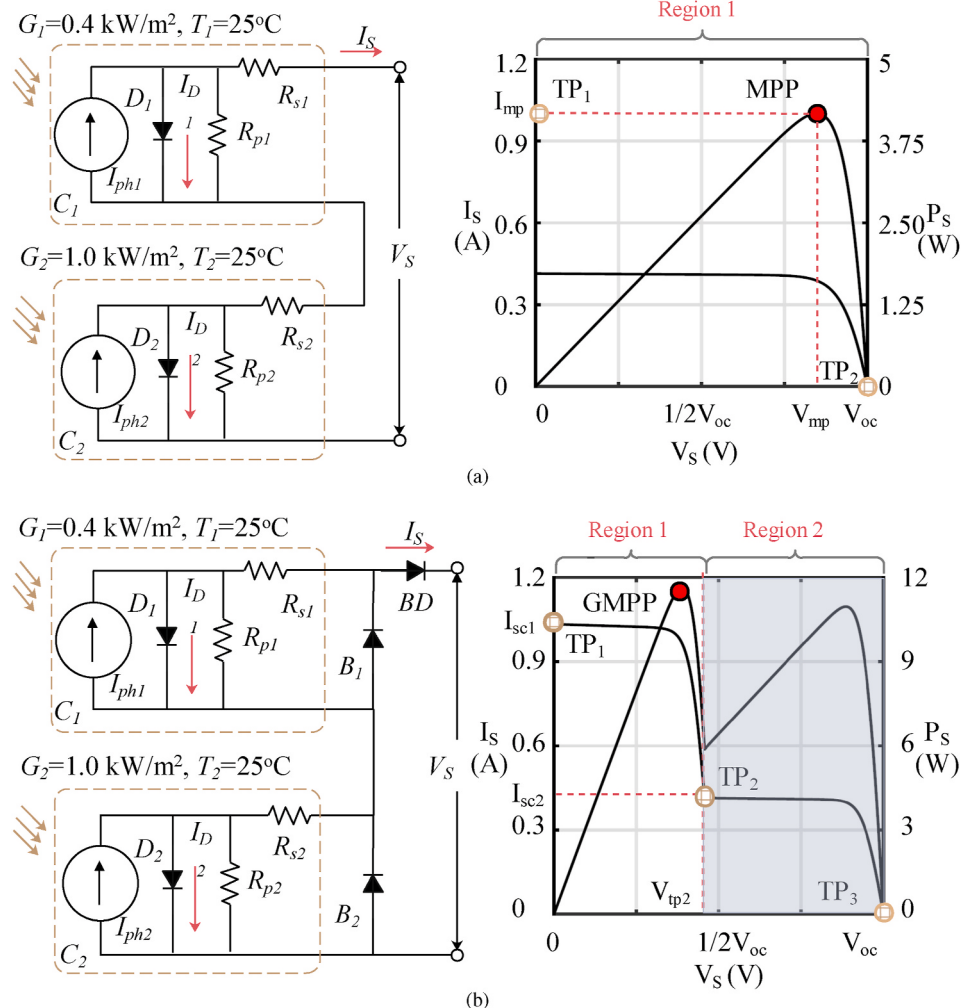


Fig. 1. Equivalent circuits and electrical characteristic curves of two PV cells: (a) without bypass diode; (b) with two bypass diodes.

- OBS2: the overall current of a PV string sinks strongly if the shaded cells are not bypassed;
OBS3: the TPs separate the I - V curve into several regions. The current at the TP is approximately equal to the corresponding short-circuit current.

3. Analytical modeling of photovoltaic strings under partial shading conditions

Most of the existing modeling methods only consider the I - V relations at different temperatures T and irradiance levels G . Let B denote the number of bypass diodes that are connected in parallel across N PV cells. This paper proposes a shading information matrix $X = \{B, N, G, T\}$, which describes partial shading conditions through shading patterns and bypass diode configurations. Given the shading information, a comprehensive analytical model is able to characterize the electrical characteristics of PV strings under PSCs and UICs. As seen in Fig. 2, the proposed modeling method obtains three components: shading information extraction (SIE), parameter estimation (PE), and analytical modeling (AM). The SIE can obtain a refined shading information matrix X' which enables the model to predict the string current in different regions. The optimal parameters $Z = \{R_S, R_P, V_B\}$ can be extracted via an FSJ algorithm. The detailed methods are introduced in the following sub-sections.

3.1. Shading information extraction (SIE)

The OBS1 indicates that raw shading location information is not sufficient to characterize the shape of I - V curves. An SIE method is therefore necessary for arranging data, and its pseudocode is shown in Algorithm 1. To detect the number of bypass diodes, a *unique* function is used to return the same data as in X , but with no repetitions. The obtained G is basically the number of steps in the I - V curve.

Another aim of SIE is to select the useful information dividing I - V regions. According to OBS2 and OBS3, the current is equal to the one generated by the shaded cells. Thus, a *for* loop to reconcile the shading information based on the I_{sc} of each cell, which can be estimated the following equation:

$$I_{sc} \cong (I_{phn} + K_I \Delta T) G / G_n. \quad (6)$$

The technical parameters $Y = \{I_{scn}, K_I\}$ are normally available in the datasheet. In X , the cell obtaining the lowest short-circuit current $I_{sc,min}$ replaces other cells that connect to the same bypass diode, and in such a way that the shading information is refined. Assume that the maximum current difference of the proposed PV model is v , the shading information can be further refined by the cells that obtain the similar I_{sc} .

Fig. 3(a) depicts an example PV string with 4-series connected cells (C_1 – C_4). A blocking diode BD is installed in series with the PV-cell string. The four cells are subjected to three different irradiance levels ($G_1 = 0.8$ kW/m²,

Algorithm 1. Shading information extraction (SIE)

Algorithm 1: Shading information extraction (SIE)

```

Input:  $X = \{B, N, G, T\}$ ,
 $Y = \{I_{scn}, K_I\}$ 
Output:  $X'$ 

▷ Find the number of irradiance levels
uniG = unique(G);
▷ Reconcile the shading information
for  $i = 1$  to  $\text{length}(uniG)$  do
    sameG = find( $G == uniG(i)$ );
    for  $j = 1$  to  $\text{length}(sameG)$  do
        Calculate the approximated  $I_{sc,i,j}$  via Eq. (6);
         $I_{sc,min,i} = \min(I_{sc,i})$ ;
        for  $j = 1$  to  $\text{length}(sameG)$  do
            Replace  $X_{i,j}$  with the one that obtains  $I_{sc,min,i}$ ;
    Merge the same elements in  $X_i$  and update  $N$ ;
    Update  $X$ ;
▷ Refine the shading information
Sort  $X$  in increasing order by the values of  $I_{sc}$ ;
for  $i = 1$  to  $\text{length}(N)$  do
    if  $|I_{sc,i} - I_{sc,i+1}| < v$  then
        Merge the items  $i$  and  $i + 1$  in  $X$ ;
        Update  $X$ ;
    Calculate  $N_B$ 
 $N_{B,1} = \text{sum}(B)$ ;
for  $i = 1$  to  $\text{length}(N)$  do
     $N_{B,i} = N_{B,1} - B_i$ ;
 $X' = \{N_B, N, G, T\}$ .

```

$G_2 = 0.4 \text{ kW/m}^2$, $G_3 = 0.4 \text{ kW/m}^2$, $G_4 = 1.0 \text{ kW/m}^2$) at three different temperatures ($T_1 = 25^\circ\text{C}$, $T_2 = 30^\circ\text{C}$, $T_3 = 31^\circ\text{C}$). The bypass diode B_1 is connected in parallel across C_1 and C_2 . According to OBS1, C_1 and C_2 are forced to carry the same current, and therefore the X_2 is replaced with the X_1 obtaining lower I_{sc} . The value of N is updated to 2 because the information of C_1 and C_2 is combined. Then, the elements X_2 can be merged into X_1 . Since the difference of I_{sc} is less than v , their current is considered the same. As seen in the last two steps in Fig. 3(b), the X_1 and X_3 are merged. Fig. 3(c) shows the corresponding two-step I-V curve of the shaded PV cell string. The X' provides sufficient environmental information for modeling, in which N_B and N represent the active and nonactive operating cells/modules in a region of the I-V curve.

$$\begin{cases} I_S = I_{ph,i} - I_{o,i} \left[\exp \left(\frac{V_{D,i}}{A_i N_{S,i} N V_{t,i}} \right) - 1 \right] - \frac{V_{D,i}}{R_{p,i}} \\ V_{D,i} = V_S + I_S R_S - V_{tp,i} + V_{BD} + N_{B,i} + V_{B,i} \end{cases} \quad (7)$$

where the V_{BD} represents the forward voltage of a blocking diode. When a PV-module string is considered, the number of series-connected PV cells is up to $N_{S,i}N$.

The pseudocode of the proposed AM method is shown in Algorithm 2. The main function Rmodel consists of four parts. The $V_{tp,i}$ and I_{sc,N_B+1} are firstly initialized. The I_{sc} of i th region can be estimated via Imodel (V_S , X , Y , Z),

Algorithm 2. Analytical modeling (AM)

Algorithm 2: Analytical modeling (AM)

```

Function Rmodel( $V_S, X, Y, Z$ ):
    >Initialization
     $V_{tp,1} = 0, I_{sc,N_B+1}=0;$ 
     $N_G = length(N)$ 
    >Predict  $I_{sc}$ 
    for  $i = 1$  to  $N_G$  do
        | Predict the  $I_{sc,i}$  via Imodel( $0, X_i, Y, Z$ );
    >Calculate  $V_{tp}$ 
    for  $i = 1$  to  $N_G$  do
        | Estimate  $V_{tps,i}$  via Vmodel( $I_{sc,i+1}, X_i, Y, Z$ );
         $V_{tp,i} = \sum_{j=1}^{N_G} V_{tps,j};$ 
    >Estimate  $I_S$ 
    for  $i = 1$  to  $N_G$  do
        | if  $V_S >= V_{tp,i}$  &  $V_S < V_{tp,i+1}$  then
             $V'_S = V_S - V_{tp,i} + V_{BD} + N_{B,i} V_{B,i}$ 
             $I_S = Imodel(V'_S, X_i, Y, Z);$ 
    return  $I_S$ 

Function Vmodel( $I_{sc}, X, Y, Z$ ):
    Define Eq. (9) as the fun_str;
    start_point= $0.8V_{oc}$ ;
     $X = newtonraphson(fun\_str, start\_point);$ 
    return  $V_{tps,i}$ 

Function Imodel( $V_S, X, Y, Z$ ):
    Define Eq. (8) as the fun_str;
    start_point= $0.8V_{oc}$ ;
     $X = newtonraphson(fun\_str, start\_point);$ 
    return  $I_S$ 

```

3.2. Analytical modeling (AM)

Based on the X^f , the proposed analytical modeling (AM) method calculates the I-V relations according to the operating point's region. As seen in Fig. 3(c), region segmentation is performed to separate two regions by three TPs in the "staircase" shape curve. The TP₁ and TP₃ are the start point and endpoint at the I-V curve. The V_{tps} represents the voltage difference between two TPs. In this example, three of four cells forward bias the parallel-connected bypass diodes, diverting the current flow of cells through themselves. All cells are reverse biased across their respective cell when the string voltage is larger than $V_{tp,2}$. The bypass diode possesses a forward voltage V_B , introducing a voltage drop in the PV system upon activation [40]. The V_B essentially affects the positions of TPs in the I-V curve Let $N_{B,i}$ denote the number of active bypass diodes in the i th ($1 < i < N_G$) region, the corresponding forward voltage is $N_{B,i}V_B$. Therefore, Eq. (4) can be rewritten as:

which was developed based on Villalva's analytical PV model [6]. Its model equations are shown in Eq. (8).

$$E_I(V_S) = I_{ph,i} - I_{o,i} \left[\exp \left(\frac{V_S + I_S R_S}{A N_{S,i} N V_t} \right) - 1 \right] - (V_S + I_S R_S) / R_p - I_S. \quad (8)$$

Since the value of I_{sc} is required, the V_S can be set to 0 V, indicating $I_{sc,i} = Imodel(0, X_i, Y, Z)$. The parameters $Z = \{R_s, R_p, A\}$ can be extracted from the measured I-V data via a PE method described in the next sub-section. I_S is the only unknown variable in Eq. (8), and its value can be obtained by finding the root of $E_I(0)$. In this paper, the Newton-Raphson algorithm is used to solve the equation.

The predicted $I_{sc,i}$ enables the algorithm to estimate $V_{tps,i}$ via Vmodel (V_S, X, Y, Z), which is a transformation form of Imodel. Its model equations are expressed as follows:

$$E_V(V_{sc,i+1}) = I_{ph,i} - I_{o,i} \left[\exp \left(\frac{V_{tps,i} + I_{sc,i+1} R_S}{A N_{S,i} N V_t} \right) - 1 \right] - V_{tps,i} + I_{sc,i+1} R_S / R_p - I_{sc,i+1}. \quad (9)$$

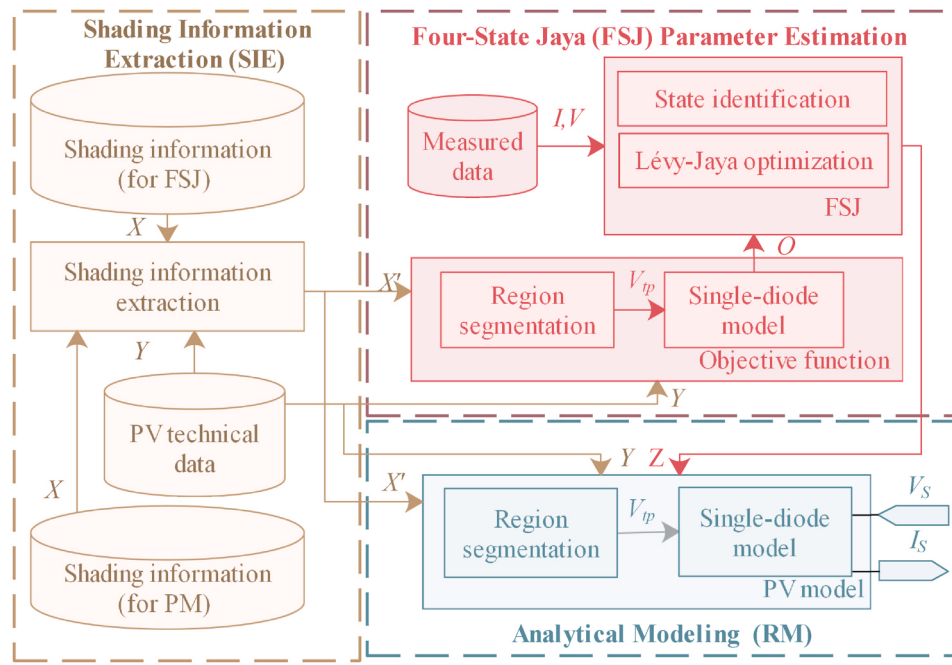


Fig. 2. Block diagram of the proposed method.

Like Imodel, the unknown variable $V_{\text{tp},i}$ is solved by the Newton-Raphson algorithm. The $V_{\text{tp},i}$ can be calculated via $V_{\text{tp},i} = \sum_{j=1}^{N_G} V_{\text{tp},j}$. The TP locus determines the I-V region that an operating point is located. It is worth pointing out that the input voltage should be adjusted due to the effect of bypass and blocking diodes. Thus, the input voltage of Imodel V_s will be given by Eq. (10), and the string current I_s is finally predicted via Imodel(V_s , X_i , Y , Z).

$$V'_s = V_s - V_{\text{tp},i} + V_{\text{BD}} + N_{\text{B},i} V_{\text{B},i}. \quad (10)$$

3.3. Four-state Jaya (FSJ) parameter estimation

A variety of optimization methods exist for extracting technical parameters that are not available in the manufacturer's datasheet [39,41]. The proposed algorithm is based on the Jaya algorithm, which is a variant of the swarm intelligence. Unlike most meta-heuristic algorithms, the Jaya algorithm does not require any hyper-parameter, which makes Jaya an attractive and easy-to-use approach [42]. Fig. 4 depicts the flowchart of the proposed method. The algorithm first initializes parameters toward the problem, e.g., the number of dimensions dim , population size pop , the maximum generation genMax , etc. The Jaya updates candidate solutions by moving them towards the best solution best_i and away from the worst solution worst_i at the i th iteration ($i \leq \text{genMax}$). Let $Z_{i,j,t}$ represent the j th ($j \leq \text{dim}$) variable of the t th ($t < \text{pop}$) candidate during the i th iteration. It is updated via Eq. (11).

$$Z_{i+1,j,t} = Z_{i,j,t} + r_{1,i,j}(Z_{i,j,best} - |Z_{i,j,t}|) - r_{2,i,j}(Z_{i,j,worst} - |X_{i,j,t}|) \quad (11)$$

where $r_{1,i,j}$ and $r_{2,i,j}$ are the two random numbers generated from a uniform distribution. In practical use, new solutions are generated around the best solution, which speeds up the local search. But sometimes, it is easy to be trapped into the local minima.

Lévy flight is a random walk that extends beyond the Brownian motion. To ensure a better exploration of the solution space, a substantial fraction of the new solutions generated by Lévy walk can be far from the current minima. Therefore, new solutions can be adjusted by

Eq. (12).

$$Z_{i+1,j,t} = Z_{i,j,t} + S_{i,j} \cdot (Z_{i+1,j,\text{randt}_1} - Z_{i+1,j,\text{randt}_2}) \quad (12)$$

where randt_1 and randt_2 are two random natural numbers less than pop . Mantegna's algorithm is used to calculate the step length $S_{i,j} = u_{i,j}/(|v_{i,j}|^{1/\beta})$. The $u_{i,j}$ and $v_{i,j}$ are drawn from normal distributions, namely $u \sim N(0, \sigma_u^2)$, $v \sim N(0, \sigma_v^2)$. The σ_v is assumed to be 1. The σ_u is given by Eq. (13):

$$\sigma_u = \left(\frac{\Gamma(1+\beta) \cdot \sin(\pi \frac{\beta}{2})}{\Gamma(\frac{(1+\beta)\beta}{2} \cdot 2^{\frac{\beta-1}{2}})} \right)^{\frac{1}{\beta}} \quad (13)$$

where the Γ denotes the gamma function $\Gamma(g) = \int_0^\infty t^{g-1} e^{-t} dt$, which is a commonly used extension of the factorial function to complex numbers.

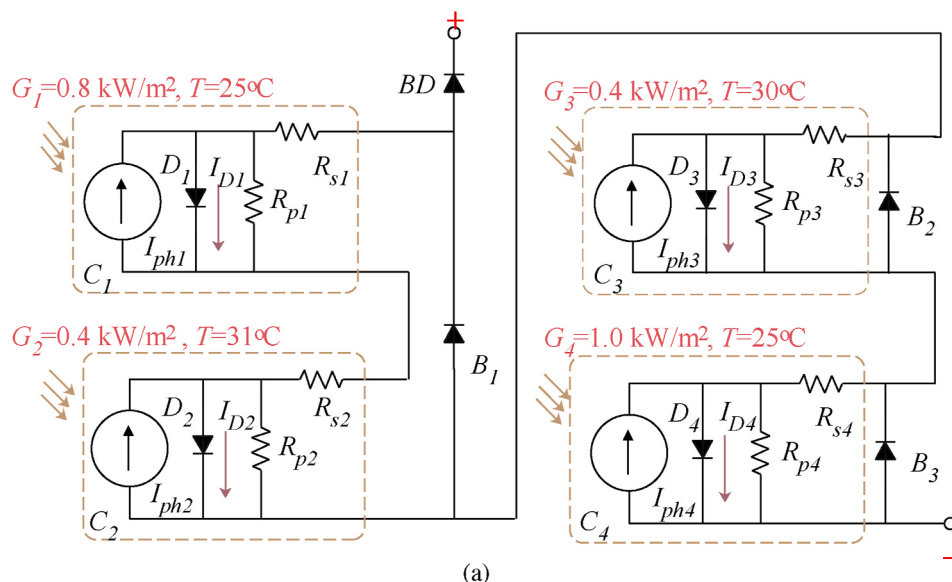
The β is a Lévy flight distribution parameter and determines the step size. To get the best performance, the β is adapted with a simple method that incorporates explorative and exploitative behaviors. As seen in Fig. 4, the optimization process can be classified into four states, which can be identified according to the values of individual difference ι and generation gap ϱ . The ι_i evaluates two candidates' differences using the Cosine similarity:

$$\iota_{i,t} = \frac{\sum_{j=1}^{N_j} \left(\frac{Z_{i,j,t}}{Z_{i,j,best}} \right) \times \sum_{j=1}^{N_j} \mathbf{I}}{\sqrt{\sum_{j=1}^{N_j} \left(\frac{Z_{i,j,t}}{Z_{i,j,best}} \right)^2} \times \sqrt{\sum_{j=1}^{N_j} \mathbf{I}^2}} \quad (14)$$

The ϱ indicates the differences of best fitness values among several iterations and checks whether a candidate is trapped in a local minimum within a window. It can be formulated by Eq. (15):

$$\varrho_i = \sum_{i=1}^{N_\omega} \text{ceil}[O(Z_{best}^i) - O(Z_{best}^{i-1})] \quad (15)$$

where N_ω is the window size. The $\text{ceil}(\cdot)$ is a function that rounds the difference between adjacent two objective values. The objective value



(a)

X	B	N	G (kW/m ²)	T (°C)	I_{sc} (A)
X_1	1	1	0.8	25	0.98
X_2	1	1	0.4	31	0.64
X_3	2	1	0.4	30	0.61
X_4	3	1	1.0	25	1.22

Reconcile

X	B	N	G (kW/m ²)	T (°C)	I_{sc} (A)
X_1	1	1	0.4	31	0.64
X_2	1	1	0.4	31	0.64
X_3	2	1	0.4	30	0.61
X_4	3	1	1.0	25	1.22

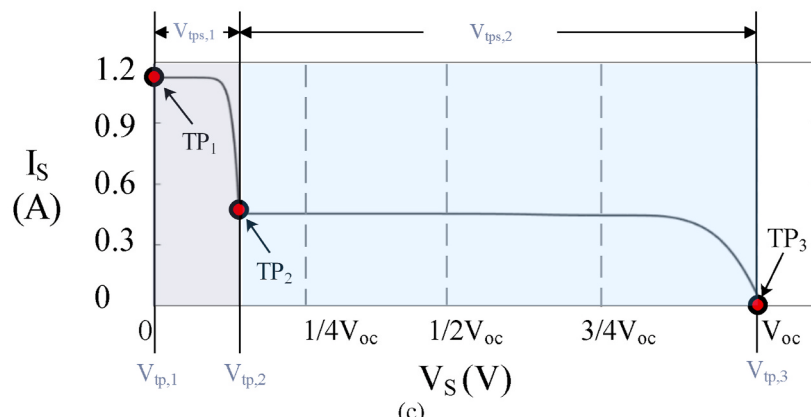
Sort&Merge

X'	N_B	N	G (kW/m ²)	T (°C)	I_{sc} (A)
X'_1	3	1	1	25	1.22
X'_2	0	3	0.4	30	0.61

(b)

X	B	N	G (kW/m ²)	T (°C)	I_{sc} (A)
X_4	3	1	1	25	1.22
X_1	2	2	0.4	31	0.64
X_3	1	1	0.4	30	0.61

(b)



(c)

Fig. 3. Shading information extraction: (a) circuit diagram of a partially shaded PV-cell string; (b) shading information extraction process; (c) the corresponding I - V curve.

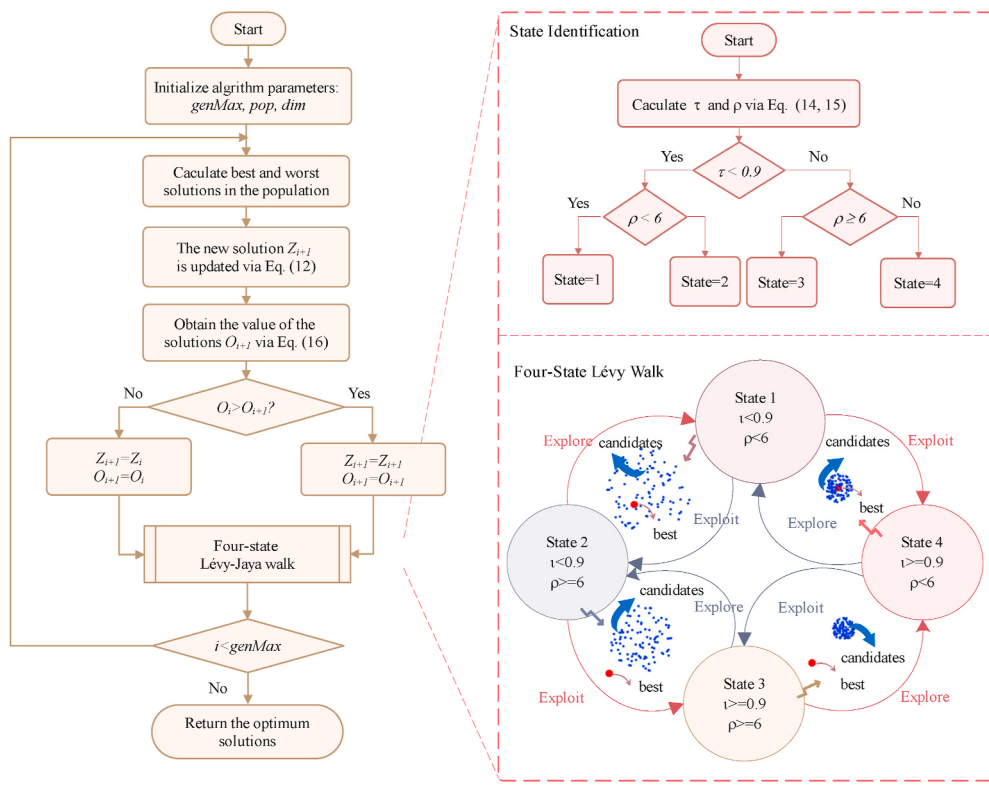


Fig. 4. Flow chart of the FSJ parameter estimation algorithm.

for the i th generation O_i can be formalized by the root means square errors (RMSE), which is given by Eq. (16):

$$O_i = \sqrt{\frac{1}{N} \sum_{r=1}^N (I_{S,i,r} - \widehat{I}_{S,i,r})^2} \quad (16)$$

where N is the number of samples; $I_{S,i,r}$ is the measured string current; and $\widehat{I}_{S,i,r}$ is its simulated value obtained by the AM.

If the new solution $Z_{i+1,j,t}$ is better than the previous one, the $Z_{i+1,j,t}$ will replace $Z_{i,j,t}$. Otherwise, the algorithm keeps the previous solution. The updated solutions will feed back to the input, which drives the candidates to get closer to the best solution and move away from the worst solution. In the four optimization states, the t of a population is small and the search scope is relatively large. The best solution is within the search scope in State 1 and State 4. The algorithm first drives the candidates to go to State 4 via explorative and exploitative behaviors, in which β is set to 1.5 and 0.75, respectively. After achieving State 4, the algorithm will probably expand the search scope to perform a global search. It will alternate the search behavior if the ϱ is not changed at six iterations. The four-state Lévy flight applies the variable step-size

method according to the optimization states. Thus the FSJ parameter estimation can essentially balance the algorithm's explorative and exploitative capabilities.

4. Results and discussions

4.1. Partially shaded PV cell string

The proposed PV model was simulated in MATLAB R2020a under Windows 10 operating system with Intel(R) Core(TM) i7-7660U with 8.00G RAM. The results were evaluated by mean squared error (MSE), root mean squared error (RMSE), and the mean absolute error (MAE). In the experiments, we applied TSM72-125M and Solartech Power SPM045P PV modules, whose technical parameters are listed in Table 1. Fig. 5 shows two testing cases in Ref. [43]. The PV cells were shaded by wax papers. A handheld pyranometer (Ambient Weather TM-206) and an infrared thermometer (HyperTough Infrared Thermometer) were used to measure the irradiance and temperature. In order to minimize the effect of irradiance and temperature variations, an electronic load (BK Precision 8500) was applied to go from open-circuit to short-circuit conditions in less than 1 min. The experiments include two cases (Case #1 and Case #2) and their shading patterns are shown in Fig. 5. The shading information matrix X was determined in accordance with the configurations of the applied PV system. Table 2 lists the arranged data obtained by the SIE process.

Before modeling, the unknown parameter Z was estimated via optimization algorithms. It is worth pointing out that different solutions may be obtained in each run. In the experiment, seven parameter estimation methods, including FSJ, Jaya [21], SA [22], PSO [23], DE [25], PS [26], and CS [29] algorithms, were evaluated. Table 3 presents the best solutions and their errors ten times for the two cases. Fig. 6 shows the corresponding RMSE values along with the number of iterations of 7 different methods. The PSO's population size, self-adjustment weight, social-adjustment, and inertia range were set to 7, 1.49, 1.49 and [0.1, 1.1], respectively. In the PS algorithm, the expansion factor is 2 and

Table 1
Technical data of the applied PV modules.

PV module	TSM72-125M	SPM045P
Cell technology	Mono-crystalline	Poly-crystalline
Maximum power	180 W	45 W
Voltage at maximum power point	35.8 V	18.3 V
Current at maximum power point	5.03 A	2.52 A
Open-circuit voltage	44.3 V	22.2 V
Short-circuit current	5.42 A	2.69 A
The number of cells	72	36
Temperature coefficient of V_{oc}	-0.34%/°C	-0.36%/°C
Temperature coefficient of I_{sc}	0.05%/°C	0.05%/°C

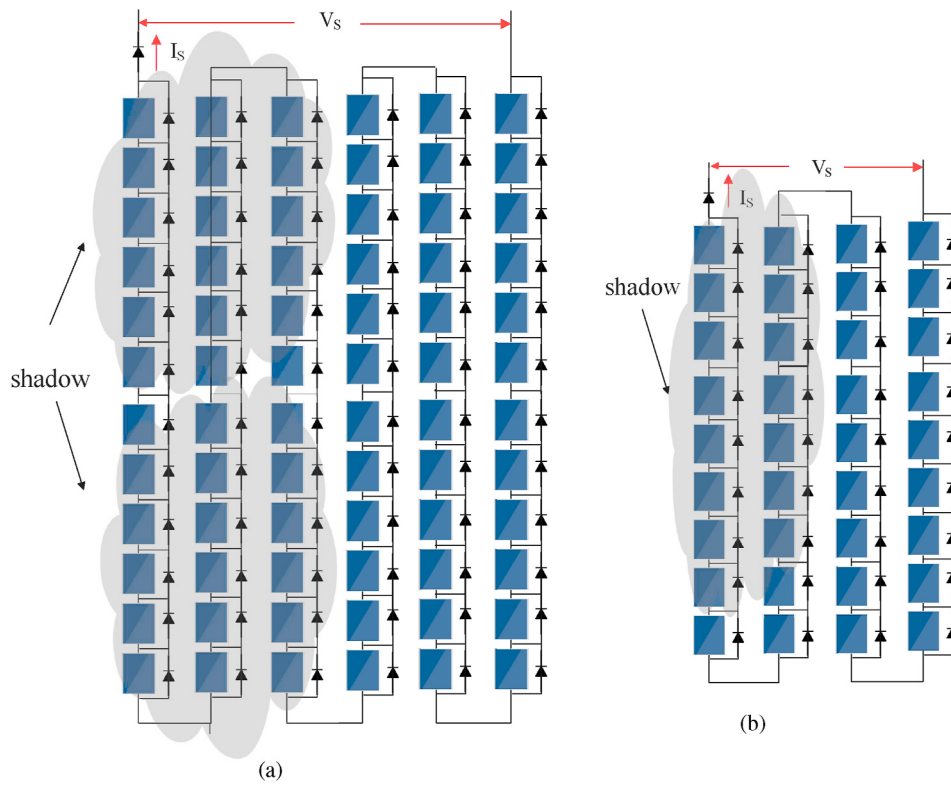


Fig. 5. Experimental setup: (a) Case #1 (TSM72-125M); (b) Case #2 (SPM045P).

contraction factor is 0.5. The upper bound lower bounds of DE's the scaling factor is 0.8 and 0.2, respectively.

Its crossover probability is 0.2. In the CS algorithm [44], the discovery rate of alien eggs/solution is set to 0.25. The maximum generation/iteration of these algorithms is set to 1000. It is observed that the Jaya and FSJ algorithms obtain the lowest MSE, RMSE and MAE. Since the proposed method improves the global search capability, the FSJ parameter estimation algorithm achieves the lowest RMSE 169 iterations ahead of Jaya algorithm. A similar trend is also seen in Case #2. The FSJ algorithm obtains the lowest errors. Although the PS algorithm shows the fastest convergence speed on SPM045P's dataset, the proposed FSJ algorithm shows the most stable optimization performance.

To evaluate the accuracy, the simulated electrical curves are compared with the results obtained from commercial simulation tools in Fig. 7. The GMPPs are also shown on these curves. In the two cases, the measured data agree well with the proposed model. Both Simulink [45] and PSIM [46] models apply the same technical parameters, but the calculated current values are slightly higher than the measured data. Due to modeling errors, the proposed model and PSIM produce a deviation of GMPP locus in Case #2. Although the predicted voltage at the GMPP is much lower than the measured data, the relative error (RE) of

Table 3
Parameters of the PV modules obtained by optimization algorithms.

Case #1	Z				Errors		
	$R_s(Q)$	$R_p(Q)$	A	$V_d(V)$	MSE (A)	RMSE (A)	MAE (A)
FSJ	0.770	2.081E+02	1.000	0.800	0.008	0.091	0.072
Jaya [21]	0.770	2.081E+02	1.000	0.800	0.008	0.091	0.072
SA [22]	0.698	2.622E+02	1.050	0.794	0.010	0.100	0.081
PSO [23]	0.000	1.017E+09	2.151	0.091	0.114	0.338	0.198
DE [25]	0.000	8.454E+02	1.613	0.764	0.043	0.208	0.148
PS [26]	0.000	3.547E+03	2.000	0.448	0.091	0.301	0.181
CS [29]	0.000	2.843E+04	2.135	0.092	0.112	0.334	0.196
Case #2	Z				Errors		
	$R_s(Q)$	$R_p(Q)$	A	$V_d(V)$	MSE (A)	RMSE (A)	MAE (A)
FSJ	0.757	4.164E+02	1.000	0.800	0.025	0.159	0.112
Jaya [21]	0.757	4.164E+02	1.000	0.800	0.025	0.159	0.112
SA [22]	0.668	2.123E+02	1.070	0.573	0.036	0.189	0.140
PSO [23]	0.297	3.236E+09	1.918	0.800	0.063	0.250	0.171
DE [25]	0.297	1.000E+10	1.918	0.800	0.063	0.250	0.171
PS [26]	0.757	4.164E+02	1.000	0.800	0.025	0.159	0.112
CS [29]	0.296	4.000E+05	1.917	0.800	0.063	0.250	0.171

Table 2
Shading information matrix for experimental case studies.

Case	Case #1 (TSM72-125 M)		Case #2 (SPM045P)	
X'	N	48	24	20
	NB	24	0	16
	G (W/m^2)	580	345	1030
	T ($^\circ\text{C}$)	39.85	47.85	14.85
				610
				38.85

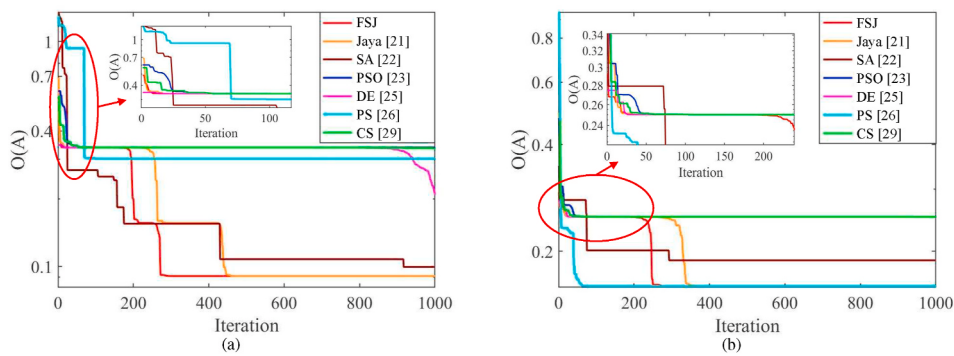


Fig. 6. The RMSE values along the number of iterations of different parameter estimation algorithms: (a) TSM72-125 M (Case #1); (b) SPM045P (Case #2).

the maximum power (MP) is only 0.050 W and it is still in an acceptable range.

4.2. Partially-shaded PV-Module string

Experiments were carried out to evaluate the proposed method's accuracy for a partially-shaded PV-module string. Fig. 8 shows the experimental setup for Case #3 and Case #4. The experiments used three-series connected poly-crystalline XHYG-10W modules operating under both UICs and PSCs. The PV cells were shaded by light films to simulate different PSCs. Temperature sensors were installed on PV modules, and the I-V curve was obtained by the PROVA-1011 PV I-V characteristic curve tester. A monocrystalline silicon PV cell 7-SSC10A-

IV was used to measure solar irradiance levels. Case #3 obtains 2 irradiance levels while Case #4 has 3 levels. The environmental conditions for the two cases are recorded in Table 4.

Optimizing by the FSJ parameter estimation algorithm, the R_s , R_p , a , and V_d are set to 0Ω , $10E+10\Omega$, 1, and 0 V, respectively. Fig. 9 shows the measured data and the simulation results. It is observed that there is a good match between the measured and the data calculated by the proposed model, indicating remarkable effectiveness in predicting I-V characteristics.

Table 5 summarizes the errors of the three models. Thanks to the parameter estimation process, the proposed model has the capability of predicting the current with the highest accuracy among the three tested models. It obtains the lowest REs at the GMPP in Case #1, #2 and #4.

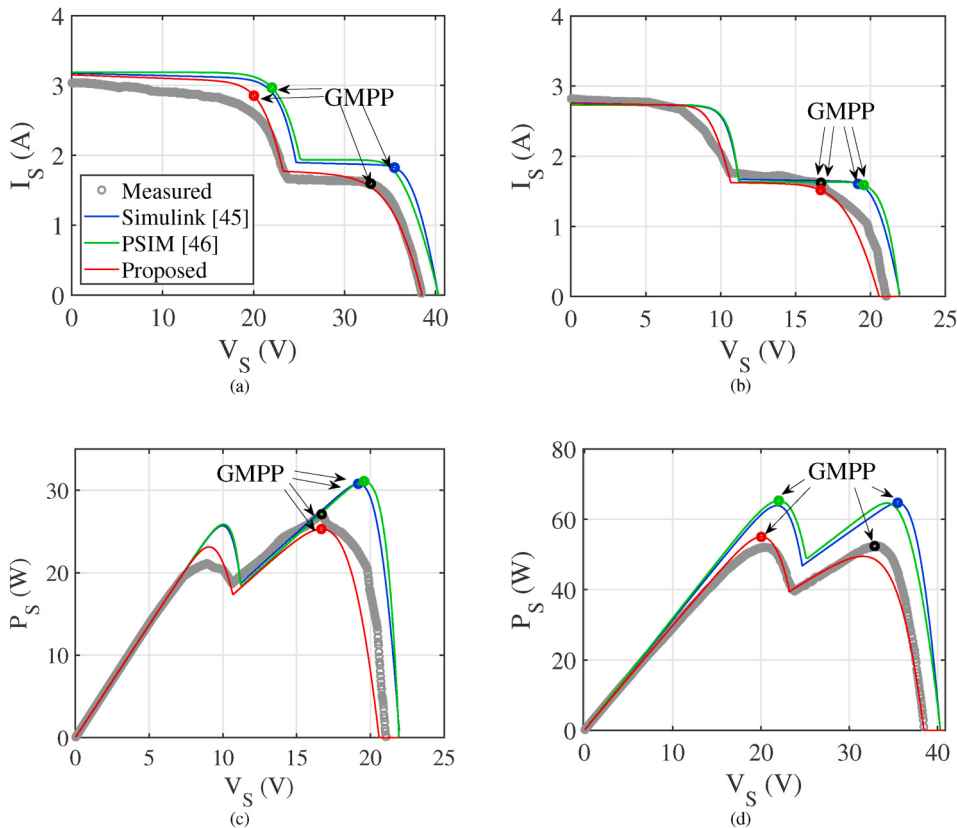


Fig. 7. The I-V characteristics of two PV-cell strings under PSCs: (a) I-V curves of the TSM72-125 M module (Case #1); (b) I-V curves of the SPM045P module (Case #2); (c) P-V curves of the TSM72-125 M module (Case #1); (d) P-V curves of the SPM045P module (Case #2).

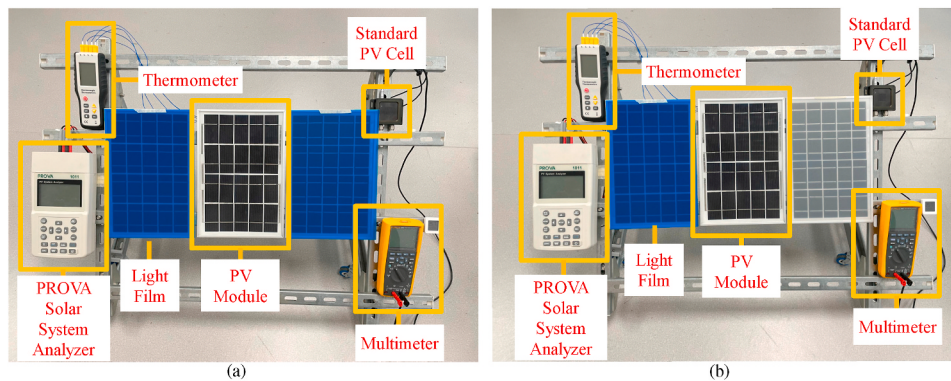


Fig. 8. Experimental setup: (a) Case #3 (XKD-50W); (b) Case #4 (XKD-50).

Table 4
Conditions of experimental case studies (Case #3 and Case #4).

Case	Case #3		Case #4	
N	1	2	1	1
X'	NB	2	0	2
G (W/m ²)	724.903	255.220	744.501	649.401
T (°)	46	31	43	49
				259.154

However, an obvious MP deviation is observed in Case #3. Two reasons caused the significant RE: 1) the measurement errors of PROVA-1011 solar *I*-*V* characteristic curve tester were higher in the low current range; 2) the objective function of the optimization drives the candidate solutions to the measured current. Due to the non-linearity of its electrical characteristics, an operating point with a low RE of current may have a high RE of power. When a high accurate prediction of GMPP locus is required, the objective function can be revised accordingly.

Fig. 10 studies the effect of bypass and blocking diodes on the electrical characteristic curves. In case #5, a PV string comprising 9 sub-strings receives uniform irradiation. The string has four power peaks in Case #6 and nine power peaks in Case #7. Each case used three different configurations of bypass and blocking diodes. In the first configuration, ideal bypass and blocking diodes were used. An ideal bypass diode and a 0.6 V-blocking diode were used in the second configuration. The last configuration used 0.6 V-bypass diodes and blocking diodes. It can be seen from Fig. 10 that the bypass diode does not affect electrical characteristic curves under uniform irradiation (SP1). Even if the blocking diode is not ideal, its effect is tiny. A remarkable power drop is seen in the low voltage range in Case #6 and #7, which indicates that non-ideal bypass and blocking diodes will decrease the output power. Fig. 11 depicts the P-V curve of PV modules with different scales ($N_G = 1 \sim 9$). The first string receives the uniform irradiation ($G = 0.2 \text{ kW/m}^2$, $N_G = 1$). The second string is twice the size

of the first one, and the new sub-string is under 0.3 kW/m^2 . In the rest cases, a new sub-string is added and each receives the irradiation 0.1 kW/m^2 higher than the previous one. All modules are working at 25°C . The output power decreases by reason of the effect of bypass and blocking diodes. The curves have been computed 10 runs. Fig. 12 shows that the average elapsed time for the proposed method is less than 0.2s. It only requires 0.137s to evaluate 29250 operating points, which is 92.08% faster than PSIM and 97.02% faster than Simulink. The test results indicate that the proposed modeling method is very effective in large-size *I*-*V* data prediction.

Table 5
Errors of different modeling methods.

Case	Errors	I			GMPP RE (W)
		MSE (A)	RMSE (A)	MAE (A)	
Case #1	Proposed	0.008	0.091	0.072	0.050
	Simulink [45]	0.183	0.428	0.380	0.235
Case #2	PSIM [46]	0.174	0.417	0.352	0.235
	Proposed	0.025	0.159	0.112	0.066
Case #3	Simulink [45]	0.105	0.324	0.208	0.136
	PSIM [46]	0.080	0.282	0.183	0.136
Case #4	Proposed	0.009	0.093	0.064	0.148
	Simulink [45]	0.022	0.148	0.083	0.048
	PSIM [46]	0.024	0.154	0.085	0.016
	Proposed	0.005	0.071	0.045	0.010
	Simulink [45]	0.010	0.215	0.243	0.215
	PSIM [46]	0.010	0.215	0.243	0.243

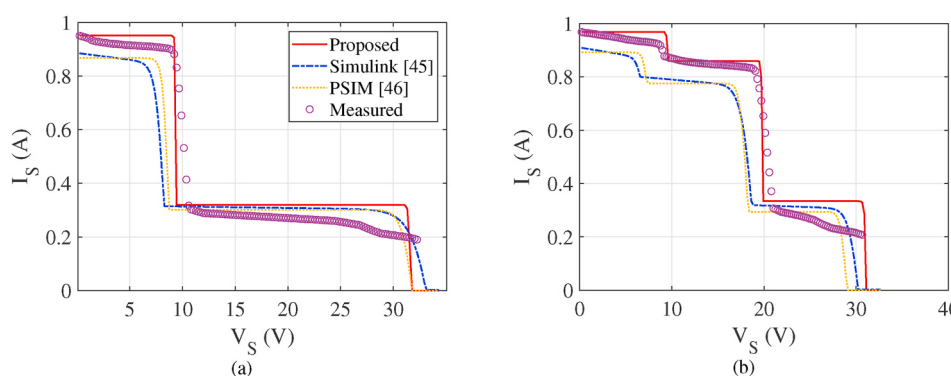


Fig. 9. The electrical characteristics of a PV-module string: (a) *I*-*V* curves for Case # 3; (b) *I*-*V* curves for Case # 4.

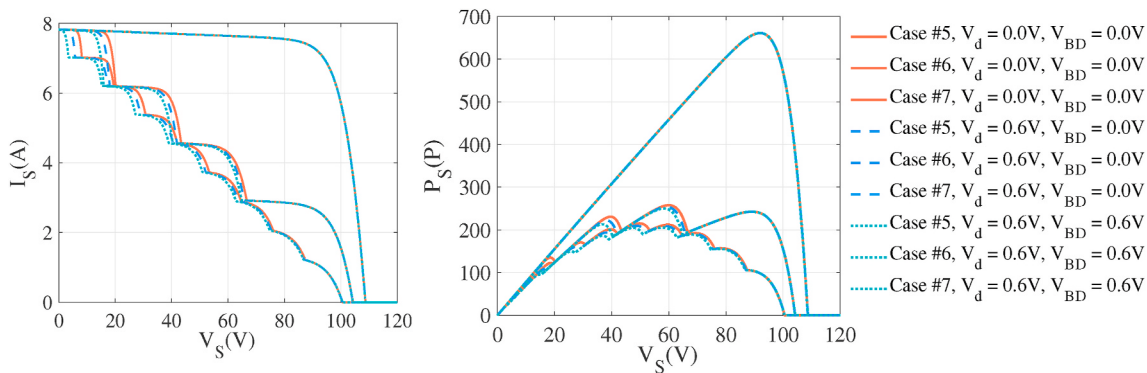


Fig. 10. The effect of bypass and blocking diodes on the electrical characteristic curves of a PV-module string: (a) I - V curves; (b) P - V curves.

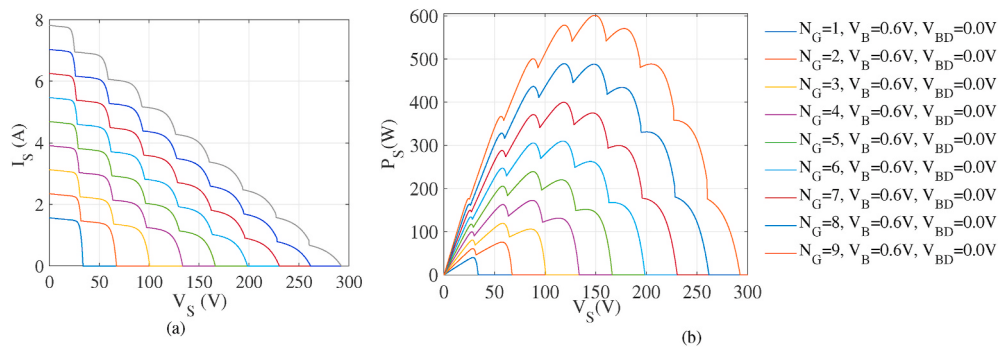


Fig. 11. The P - V characteristic curve of PV strings with different scales: (a) P - V curve; (b) the average elapsed time needed for computing P - V data.

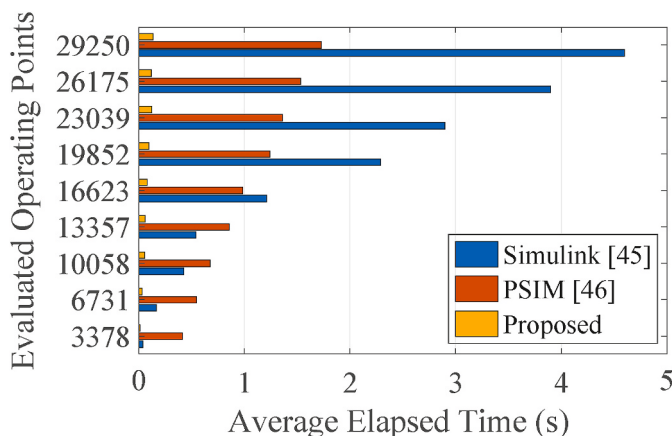


Fig. 12. The average elapsed time needed for computing P - V data.

5. Conclusion

This paper has presented an accurate and simple analytical model, in which environmental conditions and bypass diode configurations are arranged through shading information extraction. The FSJ parameter estimation algorithm enables the proposed PV model to fit a set of measured data best. In the experiments, the proposed method has been used to predict the electrical characteristic of several PV strings under different operating conditions. Results show that it improves the RMSE by at least 30% than those obtained in Simulink and PSIM. In the same test environment, it reduces the elapsed time by more than 90% compared with the other two simulation tools. The proposed modeling method can be coded in any simulation platform. It can be useful for engineers and researchers to study I - V characteristic curve of a PV string under various environmental conditions before installing a PV system.

Data availability

Datasets related to this article can be found at <https://doi.org/10.17632/yy288mjcn2.1>, an open-source online data repository hosted at Mendeley Data.

CRediT authorship contribution statement

Jieming Ma: Conceptualization, Writing – original draft. **Dou Hong:** Data curation. **Kangshi Wang:** Validation, Software. **Ziqiang Bi:** Investigation, Validation. **Xiaohui Zhu:** Writing – review & editing. **Jie Zhang:** Writing – review & editing.

Declaration of competing interest

The authors declare that they have no known competing financial interests or personal relationships that could have appeared to influence the work reported in this paper.

Acknowledgment

This research is supported by the Natural Science Foundation of China (Grant No. 62002296), the Natural Science Foundation of Jiangsu Province (Grant No. BK20200250), the Suzhou Science and Technology Project-Key Industrial Technology Innovation (Grant No. SYG202006), Qing Lan Project of Jiangsu Province, Future Network Scientific Research Fund Project (Grant No. FNSRFP-2021-YB-41), the Key Program Special Fund of Xi'an Jiaotong-Liverpool University (XJTLU), Suzhou, China (Grant No. KSF-A-19, KSF-E-65, KSF-P-02, KSF-E-54), the XJTLU Postgraduate Research Scholarship (Grand No. PGRS1906004), and the XJTLU Research Development Fund (Grant No. RDF-17-02-04).

References

- [1] J. Ma, H. Jiang, Z. Bi, K. Huang, X. Li, H. Wen, Maximum power point estimation for photovoltaic strings subjected to partial shading scenarios, *IEEE Trans. Ind. Appl.* 55 (2019) 1890–1902.
- [2] C. Perpina Castillo, F. Batista e Silva, C. Lavalle, An assessment of the regional potential for solar power generation in eu-28, *Energy Pol.* 88 (2016) 86–99.
- [3] K. Ishaque, Z. Salam, H. Taheri, S. Practice, Modeling and simulation of photovoltaic (pv) system during partial shading based on a two-diode model, *Simulat. Model. Pract. Theor.* 19 (2011) 1613–1626.
- [4] J. Ma, K.L. Man, T.O. Ting, N. Zhang, S.-U. Guan, P.W.H. Wong, Approximate single-diode photovoltaic model for efficient i-v characteristics estimation, *Sci. World J.* 2013 (2013) 7.
- [5] T.T. Yun, D. Kirschen, N. Jenkins, A model of pv generation suitable for stability analysis, *IEEE Trans. Energy Convers.* 19 (2004) 748–755.
- [6] M.G. Villalva, J.R. Gazoli, E.R. Filho, Comprehensive approach to modeling and simulation of photovoltaic arrays, *IEEE Trans. Power Electron.* 24 (2009) 1198–1208.
- [7] W. Xiao, W. Dunford, A. Capel, A novel modeling method for photovoltaic cells, in: 2004 IEEE 35th Annual Power Electronics Specialists Conference, vol. 3, 2004, pp. 1950–1956, 3.
- [8] M. Wolf, G.T. Noel, R.J. Stirn, Investigation of the double exponential in the current–voltage characteristics of silicon solar cells, *IEEE Trans. Electron. Dev.* 24 (1977) 419–428.
- [9] V. Khanna, B. Das, D. Bisht, Vandana, P. Singh, A three diode model for industrial solar cells and estimation of solar cell parameters using pso algorithm, *Renew. Energy* 78 (2015) 105–113.
- [10] J. Ahmed, Z. Salam, An accurate method for mppt to detect the partial shading occurrence in a pv system, *IEEE Trans. Ind. Inform.* 13 (2017) 2151–2161.
- [11] S. Mobailegh, J. Jiang, Modeling, prediction, and experimental validations of power peaks of pv arrays under partial shading conditions, *IEEE Trans. Sustain. Energy* 5 (2013) 293–300.
- [12] P. Rodrigo, E.F. Fernández, F. Almonacid, P.J. Pérezhigueras, A simple accurate model for the calculation of shading power losses in photovoltaic generators, *Sol. Energy* 93 (2013) 322–333.
- [13] F. Martínez-Moreno, J. Muñoz, E. Lorenzo, Experimental model to estimate shading losses on pv arrays, *Sol. Energy Mater. Sol. Cells* 94 (2010) 2298–2303.
- [14] D.D. Nguyen, B. Lehman, S. Kamarthi, Performance Evaluation of Solar Photovoltaic Arrays Including Shadow Effects Using Neural Network, ECCE, 2009, pp. 3357–3362.
- [15] S. Kanwal, B. Khan, S.M. Ali, C.A. Mehmood, M.Q. Rauf, Support Vector Machine and Gaussian Process Regression Based Modeling for Photovoltaic Power Prediction, FIT, 2005, pp. 117–122.
- [16] Z. Bi, J. Ma, X. Pan, J. Wang, Y. Shi, Anfis-based modeling for photovoltaic characteristics estimation, *Symmtry-Basel* 8 (2016).
- [17] R. Baños, F. Manzano-Agugliaro, F. Montoya, C. Gil, A. Alcayde, J. Gómez, Optimization methods applied to renewable and sustainable energy: a review, *Renew. Sustain. Energy Rev.* 15 (2011) 1753–1766.
- [18] A.A. Elbaset, H. Ali, M. Abd-El Sattar, Novel seven-parameter model for photovoltaic modules, *Sol. Energy Mater. Sol. Cell.* 130 (2014) 442–455.
- [19] T. Easwarakhanthan, J. Bottin, I. Bouhouch, C. Boutrit, Nonlinear minimization algorithm for determining the solar cell parameters with microcomputers, *Int. J. Sol. Energy* 4 (1986) 1–12.
- [20] D. Alam, D. Yousri, M. Eteiba, Flower pollination algorithm based solar pv parameter estimation, *Energy Convers. Manag.* 101 (2015) 410–422.
- [21] M. Premkumar, P. Jangir, R. Sowmya, R.M. Elavarasan, B.S. Kumar, Enhanced chaotic jaya algorithm for parameter estimation of photovoltaic cell/modules, *ISA (Instrum. Soc. Am.) Trans.* (2021).
- [22] K.M. El-Naggar, M.R. Alrashidi, M.F. Alhajri, A.K. Al-Othman, Simulated annealing algorithm for photovoltaic parameters identification, *Sol. Energy* 86 (2012) 266–274.
- [23] M. Ye, X. Wang, Y. Xu, Parameter extraction of solar cells using particle swarm optimization, *J. Appl. Phys.* (2009) 105094502.
- [24] M. Merchaoui, A. Sakly, M.F. Mimouni, Particle swarm optimisation with adaptive mutation strategy for photovoltaic solar cell/module parameter extraction, *Energy Convers. Manag.* 175 (2018) 151–163.
- [25] M.F.N. Tajuddin, S.M. Ayob, Z. Salam, M.S. Saad, Evolutionary based maximum power point tracking technique using differential evolution algorithm, *Energy Build.* 67 (2013) 245–252.
- [26] M. AlHajri, K. El-Naggar, M. AlRashidi, A. Al-Othman, Optimal extraction of solar cell parameters using pattern search, *Renew. Energy* 44 (2012) 238–245.
- [27] S. Xu, Y. Wang, Parameter estimation of photovoltaic modules using a hybrid flower pollination algorithm, *Energy Convers. Manag.* 144 (2017) 53–68.
- [28] B. Lekouaghet, A. Boukabou, C. Boubakir, Estimation of the photovoltaic cells/modules parameters using an improved rao-based chaotic optimization technique, *Energy Convers. Manag.* 229 (2021) 113491.
- [29] J. Ma, T.O. Ting, K.L. Man, N. Zhang, S.U. Guan, P.W.H. Wong, Parameter estimation of photovoltaic models via cuckoo search, *J. Appl. Math.* (2013) 1–11, 2013.
- [30] N. Rajasekar, N.K. Kumar, R. Venugopalan, Bacterial foraging algorithm based solar pv parameter estimation, *Sol. Energy* 97 (2013) 255–265.
- [31] A. Askarzadeh, A. Rezazadeh, Parameter identification for solar cell models using harmony search-based algorithms, *Sol. Energy* 86 (2012) 3241–3249.
- [32] M. Abdel-Basset, D. El-Shahat, R.K. Chakrabortty, M. Ryan, Parameter estimation of photovoltaic models using an improved marine predators algorithm, *Energy Convers. Manag.* 227 (2021) 113491.
- [33] D. Oliva, M. Abd El Aziz, A.E. Hassanien, Parameter estimation of photovoltaic cells using an improved chaotic whale optimization algorithm, *Appl. Energy* 200 (2017) 141–154.
- [34] X. Chen, B. Xu, C. Mei, Y. Ding, K. Li, Teaching-learning-based artificial bee colony for solar photovoltaic parameter estimation, *Appl. Energy* 212 (2018) 1578–1588.
- [35] K. Yu, J. Liang, B. Qu, Z. Cheng, H. Wang, Multiple learning backtracking search algorithm for estimating parameters of photovoltaic models, *Appl. Energy* 226 (2018) 408–422.
- [36] A. Pathy, H. Rezk, Parameter estimation of photovoltaic system using imperialist competitive algorithm, *Renew. Energy* 111 (2017) 307–320.
- [37] Y. Mahmoud, W. Xiao, H.H. Zeineldin, A simple approach to modeling and simulation of photovoltaic modules, *IEEE Trans. Sustain. Energy* 3 (2011) 185–186.
- [38] J. Ahmed, Z. Salam, A maximum power point tracking (mppt) for pv system using cuckoo search with partial shading capability, *Appl. Energy* 119 (2014) 118–130.
- [39] J. Ma, Z. Bi, T.O. Ting, S. Hao, W. Hao, Comparative performance on photovoltaic model parameter identification via bio-inspired algorithms, *Sol. Energy* 132 (2016) 606–616.
- [40] J. Teo, R.H. Tan, V. Mok, V.K. Ramachandaramurthy, C. Tan, Impact of bypass diode forward voltage on maximum power of a photovoltaic system under partial shading conditions, *Energy* 191 (2020) 116491.
- [41] J.J. Soon, K. Low, Photovoltaic model identification using particle swarm optimization with inverse barrier constraint, *IEEE Trans. Power Electron.* 27 (2012) 3975–3983.
- [42] R. Rao, Jaya, A simple and new optimization algorithm for solving constrained and unconstrained optimization problems, *Int. J. Ind. Eng. Comput.* 7 (2016) 19–34.
- [43] A. Xenophontos, A.M. Bazzi, Model-based maximum power curves of solar photovoltaic panels under partial shading conditions, *IEEE J. Photovolt.* 8 (2018) 233–238.
- [44] X.-S. Yang, S. Deb, Cuckoo Search via Lévy Flights, NaBIC, IEEE, 2010, pp. 210–214.
- [45] O.W. Yin, B.C. Babu, Simple and easy approach for mathematical analysis of photovoltaic (pv) module under normal and partial shading conditions, *Optik* 169 (2018) 48–61.
- [46] VeeracharyM, Psim circuit-oriented simulator model for the nonlinear photovoltaic sources, *IEEE Trans. Aero. Electron. Syst.* 42 (2006) 735–740.